

Water-stable solvent dependent multicolored perovskites based on lead bromide

Mirkomil Sharipov¹, Soojin Hwang¹, Won June Kim¹,
Bui The Huy^{1,3}, Salah M. Tawfik^{1,2} and Yong-Il Lee^{*1,3}

¹Department of Chemistry, Changwon National University, Changwon 51140, Republic of Korea

²Department of Petrochemicals, Egyptian Petroleum Research Institute, Cairo, 11727 Egypt

³Faculty of Chemical Engineering, Industrial University of Ho Chi Minh City, Ho Chi Minh City, Vietnam

(Received September 29, 2021, Revised June 2, 2022, Accepted June 9, 2022)

Abstract. The synthesis of organic and hybrid organic-inorganic perovskites directly from solution improves the cost- and energy-efficiency of processing. To date, numerous research efforts have been devoted to investigating the influence of the various solvent parameters for the synthesis of lead halide perovskites, focused on the effects of different single solvents on the efficiency of the resulting perovskites. In this work, we investigated the effect of solvent blends for the first time on the structure and phase of perovskites produced via the Lewis base vapor diffusion method to develop a new synthetic approach for water-stable CsPbBr₃ particles with nanometer-sized dimensions. Solvent blends prepared with DMF and water-miscible solvents with different Gutmann's donor numbers (D_N) affect the Pb ions differently, resulting in a variety of lead bromide species with various colors. The use of a DMF/isopropanol solvent mixture was found to induce the formation of the Ruddlesden–Popper perovskite based on lead bromide. This perovskite undergoes a blue color shift in the solvated state owing to the separation of nanoplatelets. In contrast, the replacement of isopropanol with DMSO, which has a high DN, induces the formation of spherical CsPbBr₃ perovskite nanoparticles that exhibit green emission. Finally, the integration of acetone in the solvent system leads to the formation of lead bromide complexes with a yellow-orange color and the perovskite CsPbBr₃.

Keywords: Gutmann's donor number; Lewis-base vapor diffusion; multicolor lead bromide perovskite; perovskite phase structure control; water-stable

1. Introduction

The constant advancement of technology necessitates the continuous research of new materials to develop and improve electronic devices such as photovoltaics and diodes (Nayak *et al.* 2019, Rai and Bajpai 2021, Sergeev 2021). Among various materials, lead halide perovskites have shown their potential to be a candidate for the development of light-emitting diodes and photovoltaics in recent years owing to their unique optoelectronic properties, such as their high absorption coefficient and sustained carrier diffusion (Li *et al.* 2017, Xing *et al.* 2013, Yamanouchi *et al.* 2018). Moreover, the emission wavelength of metal halide perovskites can be tuned accurately either by controlling the size of the nanocrystals (NC) or by using appropriate mixtures of various halides (Akkerman *et al.* 2015, Kovalenko *et al.* 2017, Shamsi *et al.* 2019). The combination of bromide and chloride, for example, contributes to the formation of blue-emitting perovskites, whereas the combination of bromide and iodide allows red-emitting perovskites to be formed. The observed blue- and red-shift in mixed halides is attributed to the tuning of the bandgap (Sadhanala *et al.* 2014). These mixed-halide perovskites, unfortunately, are adversely affected by non-radiative

recombination, resulting in low photoluminescence quantum efficiencies (PLQEs). In addition, photoinduced phase segregation is usually observed in mixed-halide perovskites, which can affect their long-term efficiency (Li *et al.* 2016, Yoon *et al.* 2016). This concern was addressed by synthesizing spectrally stable blue-emitting films of separated nanoplatelets of Cs₄PbBr₆ under Cs-rich conditions in the presence of moisture (Zou *et al.* 2019).

The intrinsic ionic properties of inorganic and organic perovskites, on the other hand, complicates their long-term efficiency and makes them particularly unsuitable for applications requiring the use of water or polar solvents, such as analytical sensors. To date, several approaches involving the use of surface passivation to increase the stability of perovskites have been researched, including organic Lewis bases (thiophene and pyridine) (Noel *et al.* 2014), polymers (Han *et al.* 2022, Li *et al.* 2018), and metal oxides (SiO₂, Al₂O₃, and Ta₂O₅) (Hu *et al.* 2018, Huang *et al.* 2016, Lojudice *et al.* 2017, Zhong *et al.* 2018). An alternative approach was the synthesis of organic-inorganic hybrid and fully inorganic perovskites *via* the Lewis base vapor diffusion (LBVD) method, which allowed the surface to be pacified with lead hydroxide (Pb(OH)₂), and which granted the perovskites six months of stability in water (Jana and Kim 2018). Other methods that were employed to produce the water-stable methylammonium lead bromide perovskite (MAPbBr₃) entailed surface passivation with lead bromide hydroxide (PbBr(OH)) using two different approaches: the first is based on dissolving the precursors in dimethylformamide (DMF) and ammonia solution

*Corresponding author, Professor
E-mail: yilee@changwon.ac.kr

($\text{NH}_3 \cdot \text{H}_2\text{O}$) followed by water treatment (Liu *et al.* 2020), whereas the second approach is based on N-donor imidazole derivatives (Lin *et al.* 2020).

Recent studies have reported the influence of solvent interaction with the precursor on the formation of lead halide perovskite by varying solvent parameters such as the dielectric constant (Rahimnejad *et al.* 2016, Saidaminov *et al.* 2015) or Mayer bond order (Stevenson *et al.* 2017). The polarity of the solvent participating in the synthesis reaction was suggested to be a determining factor for coordination with the lead halide salt, thereby resulting in the formation of lead-solvent complexes (Rahimnejad *et al.* 2016). On the other hand, Hamill *et al.* (2018) investigated Gutmann's donor number (D_N) of solvents as a parameter that influences the ability of Pb^{2+} to coordinate with iodine during the synthesis of MAPbI_3 . Their results showed that solvents with a low D_N are less inclined to interact with Pb^{2+} , thus promoting the complexation of Pb^{2+} with iodide ions, whereas solvents with a high D_N showed the opposite behavior because of stronger coordination with Pb^{2+} ions.

In this work, we present for the first time a simple synthetic method that enables the phase control of lead bromide perovskite nanomaterials via variation of solvent blends and prolonged reaction in LBVD system. We sought to solvate lead (II) bromide (PbBr_2) complexes by introducing these mixed solvents that contain DMF to slow the crystallization process, thus minimizing the size of the formed nanoparticles. Interestingly, mixtures of DMF with the water-miscible solvents: isopropanol, dimethyl sulfoxide (DMSO), and acetone, which have different D_N values, directly influence the strength of interaction between Pb^{2+} and bromide, resulting in the formation of lead bromide particles with different properties. These three solvents were mixed with DMF in a ratio of 3:1 to allow thorough dissolution of the precursor salts, which were then further reacted in the presence of a vaporized Lewis base to form nanoparticles that emit different colors when exposed to UV radiation: blue-emitting particles (BEPs), green-emitting particles (GEPs), and yellowish-orange emitting particles (YEPs). The formed nanoparticles had good water stability with high photoluminescence quantum yields (PLQYs) of 49.4%, 66.6%, and 35.5% for BEPs, GEPs, and YEPs, respectively. The lead hydroxide and lead bromide hydroxide shells that were formed in this way granted excellent stability and solvation properties to the formed nanoparticles. Structural analysis suggested that the observed color shifts are dictated by the different phases of cesium lead bromide particles. We propose that BEPs are formed as the $\text{MA}_{4-x}\text{Cs}_x\text{PbBr}_6$ phase under methylammonium-rich conditions, and that these particles are protected and solvated by $\text{Pb}(\text{OH})_2$, which forms a shield, resulting in blue emission. In contrast, the green color emission of GEPs originates from particles in the CsPbBr_3 phase coated with $\text{Pb}(\text{OH})_2$. Finally, the yellowish-orange emission was attributed to lead bromide complexes.

2. Experimental section

2.1 Materials and methods

Lead (II) bromide (PbBr_2) was purchased from Fisher

Chemical. Cesium carbonate (Cs_2CO_3) (99.9%) and DMF (HPLC grade) were purchased from Alfa Aesar. Acetone (Emsure® grade) was purchased from Merck Millipore (Sigma Aldrich), and DMSO was purchased in Sigma Aldrich. Methylamine (40% solution in water) and 2-propanol (HPLC grade) were purchased from Daejung Chemicals. Hydrobromic acid (HBr) (48%) was purchased from Fujifilm Wako Chemicals. Ethyl acetate was purchased from Samchun Chemicals. All chemicals and reagents were used directly without further purification. In all experimental procedures, deionized water of Milli-Q grade was used.

2.2 Characterization

The photoluminescence (PL) intensity measurements were carried out using an FP-6500 spectrofluorometer (Jasco, Japan) with a quartz cuvette with a path length of 1 cm. Field-emission scanning electron microscopy (FE-SEM) measurements were acquired using a CZ/MIRA LMH FE-SEM microscope. Transmission electron microscopy (TEM) images were recorded on a JEM-2100F transmission electron microscope (JEOL, Tokyo, Japan) operating at 200 kV. Dynamic light scattering (DLS) analysis was carried out using a Zetasizer Nano ZS90 apparatus (Malvern Instruments, Worcestershire, U.K.) The absorption spectra were obtained using an Agilent 8543 UV/Vis spectrophotometer (Agilent, USA). Diffusion reflectance spectra of films were acquired using V-670 UV/Vis spectrophotometer (Jasco, Japan). Fourier transform infrared (FTIR) spectra were recorded on an FT/IR-6300 Fourier Transform Infrared Spectrometer (Jasco, Japan). Centrifugation was carried out using a LaboGene 1580R centrifugal separator (LaboGene, Korea). X-ray photoelectron spectroscopy (XPS) were carried out using using a K-Alpha system (Thermo Scientific). X-ray diffraction (XRD) was carried out on a Bruker D8 Discover diffractometer with $\text{Cu K}\alpha$ radiation ($\lambda = 0.1542$ nm). Samples were fixed to a glass substrate for the analysis.

2.3 Synthesis of multi-colored lead bromide particles

Two acidic precursors were prepared by dissolving 1.5 mmol Cs_2CO_3 (500 mg) in 3 mL HBr (denoted as solution A) and 2.6 mmol PbBr_2 (1 mg) in 2 mL HBr (denoted as solution B). Afterward, solution A (300 μL) and solution B (300 μL) were added to a mixture of 1 mL of DMF and 3 mL of a miscible solvent (DMSO, acetone, or isopropanol) as summarized in Table 1. Each of these three vials was placed in a larger vial containing 25 mL MA and allowed to react for seven days at room temperature, after which the reaction mixtures were centrifuged at 3000 rpm to remove non-luminescent microparticles that had formed. The supernatant was poured into ethyl acetate (1:10), and after shaking for one minute, the ethyl acetate layer was carefully removed. This step allowed the removal of excess DMF and organic solvents that solvated the nanoparticles. The lower layer was again poured into ethyl acetate (1:10) to precipitate the nanoparticles. Finally, the nanoparticles were collected by centrifugation at 4000 rpm for 15 minutes and dried at 60 °C overnight.

Table 1 The ratio of solvents

Vials	DMF	Acetone	DMSO	Isopropanol	Color
Sample 1	1 mL	0	0	3 mL	Blue
Sample 2	1 mL	0	3 mL	0	Green
Sample 3	1 mL	3 mL	0	0	Yellow-orange

2.4 Preparation of multi-colored lead bromide particles @PVDF-HFP films

The Poly(vinylidene fluoride-co-hexafluoropropylene) (PVDF-HFP) films were prepared by dissolving 1 g of PVDF-HFP in DMF at 80 °C for 1 hour. Subsequently, the cesium lead bromide particles dispersed in 1 mL of DMF were mixed with 9 mL of the prepared PVDF-HFP solution. The final solution was vortexed for 5 minutes, drop-casted on glass cover slides, and dried in the oven preheated at 60 °C for 1 hour. The formed films were then immersed in DI water for 30 minutes.

2.5 Computational details

First-principles calculations were performed using density functional theory (DFT) implemented in Quantum Espresso code. (Giannozzi *et al.* 2009, 2017) The generalized gradient approximation (GGA) designed by Perdew, Burke, and Ernzerhof for solid systems (PBEsol) was used for the exchange-correlation functional. (Perdew *et al.* 2008) The plane waves for valence electrons were expanded up to a kinetic energy cutoff of 70 Ry, and the interactions between valence electrons and the core electrons were effectively treated using a scalar-relativistic version of optimized norm-conserving pseudopotentials in the PsDojo database. (van Setten *et al.* 2018) Brioulline-zone integration was accomplished with a Γ -centered k -grid of $2 \times 2 \times 2$. The electronic total energy was converged until the total energy difference between electronic steps became smaller than 1.0×10^{-8} Ry, and the geometry was optimized until all atomic forces became smaller than 1.0×10^{-4} Ry/Bohr. The optimized lattice parameters of Cs_4PbBr_6 (rhombohedral unit cell, space group $R\bar{3}c$) are $a = 13.58 \text{ \AA}$ and $c = 17.15 \text{ \AA}$ and agree with those in previous reports. (Jung *et al.* 2019).

3. Results and discussion

In recently reported work, the synthesis of lead halide perovskite by the LBVD approach made it possible to control the formation of the peripheral layer of the perovskite such that the geometry is octahedral. In addition, the formation of the $\text{Pb}(\text{OH})_2$ shell enhanced the stability of the perovskite toward aqueous media (Jana and Kim 2018). However, the main drawback of this method is the large size of the synthesized particles. Combining the Cs_2CO_3 and PbBr_2 precursor solutions yields a yellow precipitate that comprises micrometer-sized particles, which further serves as a base for the formation of the perovskite particles. The solubility of the precursors in suitable polar

solvents, such as DMF, DMSO, and acetone, encouraged us to integrate the solvents to form solvent mixtures to impede the aggregation of the precursors to form large particles at the beginning of the reaction (Fateev *et al.* 2020, Li *et al.* 2018, Shamsi *et al.* 2019, Stevenson *et al.* 2017). Thus, precursor solutions in mixed solvents with different D_N values, DMF/isopropanol (sample 1), DMF/DMSO (sample 2), and DMF/acetone (sample 3), were reacted in the presence of methylamine vapor for seven days (Fig. 1(a) and Table 1). The multi-colored perovskite particles that were formed were collected by precipitation in excess ethyl acetate to yield solid particles with bluish green, green, and dark yellowish-orange emissions, as illustrated in Fig. 1b. After dispersion in water, the emissions of these nanoparticles were sky blue, green, and yellowish-orange, respectively (Fig. 1(b)).

To understand the observed color shifts, photoluminescence spectroscopy was used to characterize all three samples before and after precipitation. As shown in Fig. 2(a), before precipitation, the three different samples had broad emission spectra with peaks located at 450 nm, 541 nm, and 605 nm for BEP, GEP, and YEP, respectively. Interestingly, washing and precipitation with ethyl acetate caused YEP to undergo blue shift from 605 nm to 562 nm with a shoulder at around 600 nm. Upon redispersion of the YEP nanoparticles in water, they exhibit a slight blue shift with a sharper emission peak. The ability of lead to form fluorescent complexes such as PbBr_3^- or $\text{Pb}_4\text{Br}_{11}^{3-}$ clusters in appropriate solvent such as polyethylene glycol or acetone were reported in previous works (Chin *et al.* 2020, Dutta and Perkovic 2002, Li *et al.* 2009). Moreover, these complexes have emission peak located at around 600 nm. Thus, the observed blue shift in YEP indicates the formation of lead complexes during LBVD synthesis and their removal during the precipitation step. In contrast, the color of the BEP emission shifted from sky blue to bluish-green upon precipitation, which corresponds to a red shift of ~ 50 nm (Figs. 1(b) and 2(b)). However, the redispersion of BEP in water led to the recovery of its native sky-blue emission with an emission peak located at 440 nm. Finally, the GEP nanoparticles did not exhibit a significant color change with a slight blue shift. All samples were further characterized via UV/Vis spectroscopy, XRD, XPS, FTIR, and FE-SEM techniques to understand the structural and morphological differences between the formed nanoparticles that dictate the color changes. Considering the changes in the emission color observed in the different states, particularly in the case of BEPs and YEPs, the nanoparticles were loaded into a PVDF-HFP film (Figs. 1(c) and 2(c)). This allowed their separate states to be preserved, thus limiting the color changes in the solid state. Moreover, the photoluminescence intensity of BEP- and GEP-loaded PVDF-HFP films exposed to water was found to increase, as shown in Fig. 1(c).

The normalized UV/Vis absorption spectra of dispersions of the perovskite particles in water showed that BEPs absorb at 335 nm (Fig. 2(d)). In previously reported studies, the absorption peak located at ~ 320 nm was ascribed to the formation of the Cs_4PbBr_6 phase under Cs-rich conditions (Liu *et al.* 2017, Wu *et al.* 2017, Zou *et al.* 2019). Similarly, the absorption peaks of GEPs are located at 291 nm and

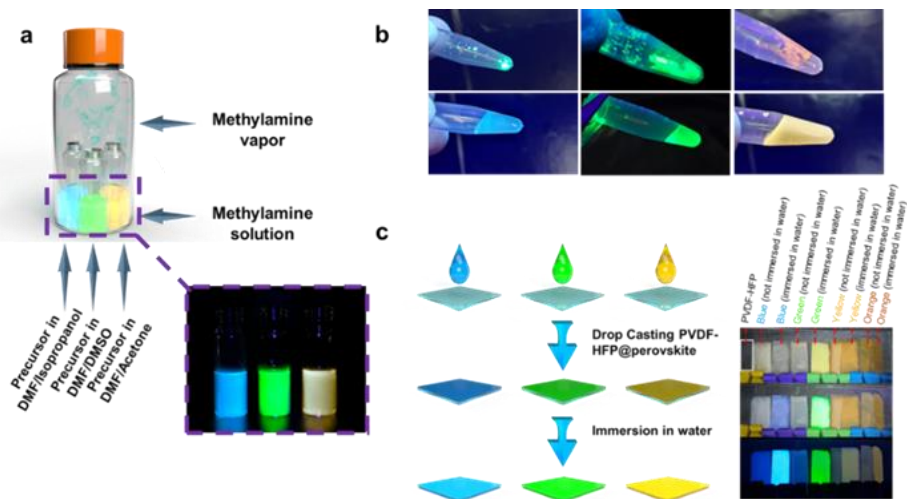


Fig. 1 Solvent-dependent LBVD synthesis approach for the preparation of multi-colored perovskite nanoparticles (a) Photographic images of multi-colored perovskite particles under UV light (365 nm) in the solid state (upper row) and dispersed in water (lower row) (b) Illustration of the process to prepare the multi-colored PVDF-HFP films (left) and photographic images of the prepared films (right) (c) The images in the top row were captured under ambient light without UV light, those in the middle row were captured under ambient light with UV illumination; The images in the bottom row were captured in the dark under UV light; Note: the UV source was located at a distance of 10 cm

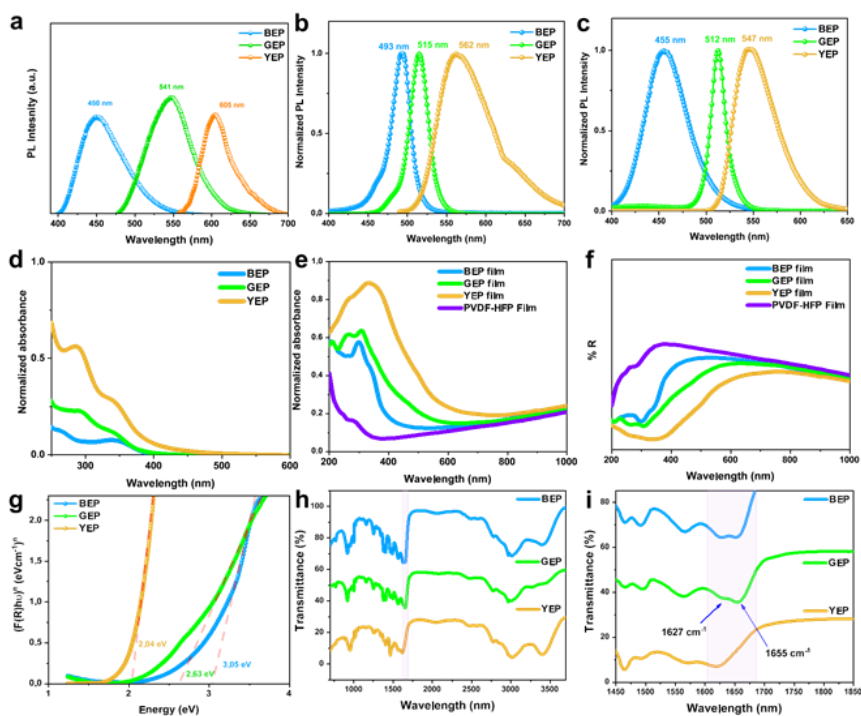


Fig. 2 Photoluminescence spectra of BEP, GEP, and YEP before the precipitation by ethyl acetate (a) Normalized photoluminescence spectra of precipitated multi-colored perovskite particles (b) and multi-colored perovskite@PVDF-HFP films (c) Normalized absorption spectra of perovskites dispersed in water (d) and perovskite@PVDF-HFP films (e) Reflectance spectra of perovskite@PVDF-HFP films (f) Estimation of band gap energy using the Kubelka-Munk function (g) FTIR spectra of BEP, GEP, and YEP particles; FTIR spectra confirm the presence of DMF and MA in all three nanoparticles (h)-(i)

334 nm; however, the absorption spectrum is broadened in comparison. Finally, YEPs absorb at 286 nm and 338 nm and their spectra are the most broadened. Analysis of the absorbance of the multi-colored perovskite-loaded films *via* diffuse reflectance spectroscopy, shown in Fig. 2(e), revealed

similar results. The BEPs had an absorption peak at 300 nm, with a shoulder located at 338 nm. On the other hand, the spectrum of the GEPs was similar but less well resolved. Finally, the absorption spectrum of the YEPs was the broadest, with maximum absorbance at 337 nm.

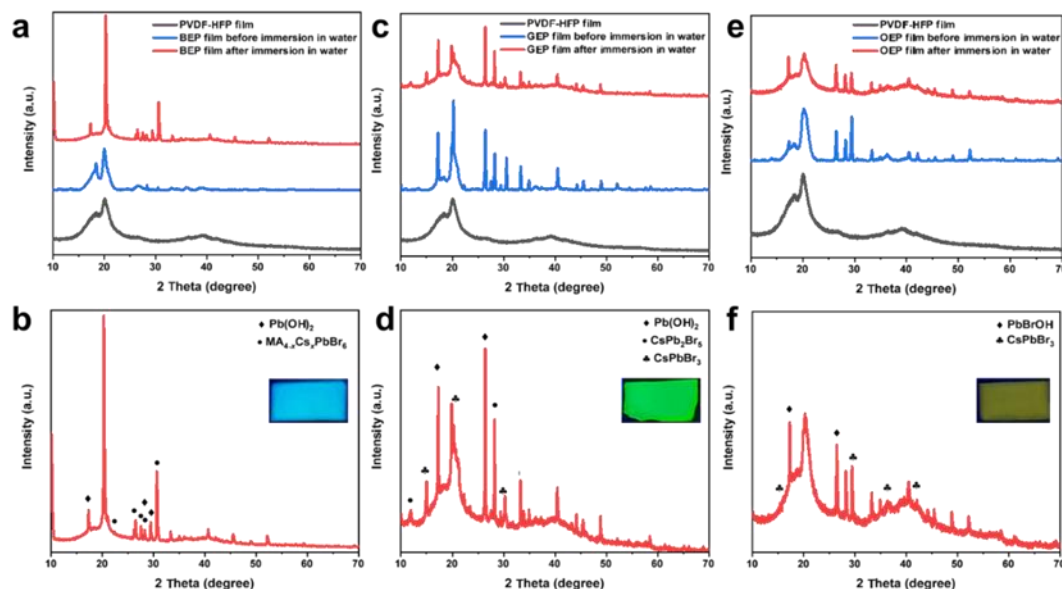


Fig. 3 XRD patterns of blue-emitting film compared with PVDF-HFP films and BEP@PVDF-HFP films (a)-(b). XRD patterns of green-emitting film compared with PVDF-HFP films and GEP@PVDF-HFP films (c)-(d). XRD patterns of orange emitting film compared with PVDF-HFP films and YEP@PVDF-HFP films (e)-(f). Note: the blue and red patterns correspond to the multi-colored PVDF-HFP films containing the lead bromide particles before and after immersion in water, respectively

Using absorption, reflectance, and Kubelka-Munk spectra, the bandgaps of the YEP-, GEP-, and BEP-PVDF-HFP films were estimated to be 2.04, 2.63, and 3.05 eV, respectively (Figs. 2(e)-2(g)). Importantly, the BEP and GEP films have indirect bandgaps whereas the YEP film has a direct bandgap. Previous work reported a large bandgap of 3.95 eV for Cs_4PbBr_6 , assuming UV emission (Akkerman *et al.* 2018). However, in practice, the emission wavelengths of the majority of the reported Cs_4PbBr_6 perovskites were located in the range of 515 to 524 nm. Two hypotheses were proposed to explain the origin of the green emission: (i) the existence of the CsPbBr_3 phase that was inserted in the Cs_4PbBr_6 matrix, thus down-converting the emitted light (Quan *et al.* 2017, Riesen *et al.* 2019, Xu *et al.* 2017, Xuan *et al.* 2018), and (ii) intrinsic defects within the wide bandgap, for example, caused by bromine vacancies (Akkerman *et al.* 2017, De Bastiani *et al.* 2017, Seth and Samanta 2017, Yin *et al.* 2018). On the other hand, the bandgap of GEPs was blue-shifted compared to that reported for CsPbBr_3 perovskite nanoparticles. Recently, a study by Ying *et al.* (2020) showed a slight blue shift in the photoluminescence of CsPbBr_3 micro-/nanorods coated with $\text{Pb}(\text{OH})_2$. Moreover, they also suggested that residual MA^+ may cause a photoluminescence blue shift. To confirm the presence of residual MA^+ cations, we conducted an FTIR analysis. As shown in Figs. 2(h) and 2(i), the MA^+ vibrational modes for C—N rocking and C—N stretching are located at $\approx 920\text{ cm}^{-1}$ and $\approx 1000\text{ cm}^{-1}$, respectively. Moreover, the C = O bond stretching vibration located at 1671 cm^{-1} in bare DMF solvent appears at $\approx 1655\text{ cm}^{-1}$ for BEPs and GEPs, whereas YEPs do not exhibit this vibration. Finally, the estimated, red-shifted band gap for YEPs can be explained *via* the formation of the lead

bromide complex, which has an emission peak at 610 nm (Chin *et al.* 2020, Dutta and Perkovic 2002).

After evaporation of the DMF solvent, the formed multi-colored films were immersed in water for 30 minutes. Interestingly, the GEP and BEP films showed substantial photoluminescence enhancement after incubation in water, whereas the YEP film did not show significant enhancement (Fig. 1(c)). To gain insight into the color difference of the emissions and the enhancement of the emission after exposure to water, we carried out XRD analyses of the PVDF-HFP films loaded with BEPs, GEPs, and YEPs before and after immersion in water (Fig. (3)). As shown in Figs. 3(a) and 3(b), immersion of the BEPs in water strongly enhanced the peaks at $2\theta=17^\circ$ and $2\theta=29^\circ$, which are attributed to $\text{Pb}(\text{OH})_2$, whereas the remaining peaks correspond with those of the Cs_4PbBr_6 phase [mp-23436, Materials Project data repository]. The reformation of the $\text{Pb}(\text{OH})_2$ shell, which apparently was removed at high temperatures during the film preparation process, explains the photoluminescence enhancement after immersion in water. Similar PL enhancement was observed by Shan's group, who discovered that $\text{MAPbBr}_3@ \text{PbBr}(\text{OH})$ has the ability to enhance its photoluminescence properties in water (Liu *et al.* 2020).

On the other hand, the XRD patterns in Figs. 3(c) and 3(d), which correspond to the GEP film, show that water immersion induces a phase transformation from CsPb_2Br_5 to CsPbBr_3 by the apparition of the peak at $2\theta=15^\circ$. This observed phase transformation induced by the removal of PbBr_2 explains the substantial color enhancement. However, the peaks corresponding to CsPb_2Br_5 are still present in small quantities [mp-1238811, Materials Project data repository], indicating that residual CsPb_2Br_5 particles

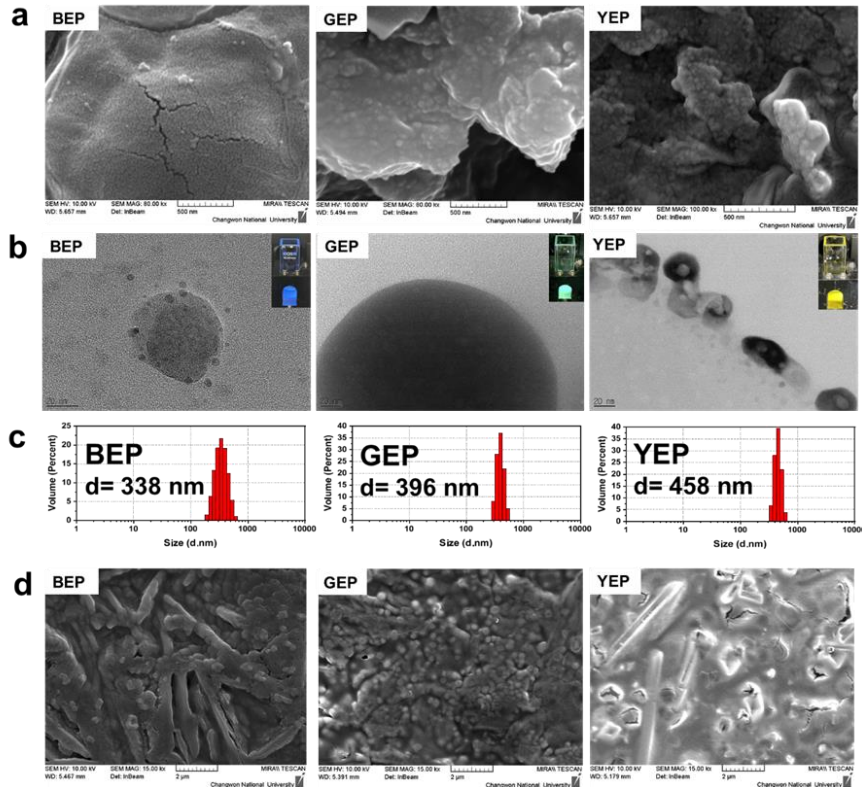


Fig. 4 FE-SEM images of BEPs, GEPs, and YEPs in the PVDF-HFP films (a) TEM images of BEPs, GEPs, and YEPs (b) Hydrodynamic size distribution of BEPs, GEPs, and YEPs determined *via* DLS (c) FE-SEM images of all three nanoparticles in the aggregated state. (d)

located inside the hydrophobic polymer cannot be transformed into CsPbBr_3 by releasing PbBr_2 . Moreover, the GEP films also exhibit peaks at $2\theta=17^\circ$ and $2\theta=29^\circ$, which are attributed to Pb(OH)_2 and allow emission enhancement and high stability in water and polar solvents. Finally, the XRD results of the YEP film showed that the peaks corresponding to PbBrOH located at $2\theta=17^\circ$ and $2\theta=26^\circ$ were enhanced (Figs. 3(e) and (f)). In addition, the XRD results indicate a small amount of the CsPbBr_3 phase by the apparition of the peak at $2\theta=15^\circ$, thus explaining the broad emission of YEP.

The morphology and sizes of the BEPs, GEPs, and YEPs were investigated *via* FE-SEM and TEM. As shown in Fig. 4(a), the BEPs incorporated in the PVDF-HFP film are smaller than 50 nm, whereas the GEPs and YEPs are slightly larger in the film, ranging from 50 nm to 100 nm. All three types of nanoparticles loaded in the PVDF-HFP films were confirmed to have spherical shapes and uniform sizes. To further investigate the morphology of the multi-colored particles before they were loaded into the PVDF-HFP film, their TEM images were analyzed (Fig. 4(b)). These TEM images confirmed that the BEPs are well-separated nanoplatelets in the solvated state with an average size smaller than 50 nm, whereas the GEPs are spherical nanoparticles with a size exceeding 100 nm. Finally, the YEPs are spherical nanoparticles mixed with nanoplatelets with a size smaller than 50 nm.

The small size and surface passivation by Pb(OH)_2 and PbBrOH conferred upon these nanoparticles the unique

characteristic of being instantly solvated by water. Therefore, the hydrodynamic size of the multi-colored lead bromide perovskite nanoparticles in the solvated state was measured *via* the dynamic light scattering technique. As shown in Fig. 4(c), the hydrodynamic size of these particles is relatively much larger than that of the nanoparticles observed *via* FE-SEM and TEM owing to the excellent solvation by water. The FE-SEM images of the BEP, GEP, and YEP nanoparticles after precipitation without incorporation into the PVDF-HFP film showed that BEPs are more likely to occur in the form of aggregated nanoplatelets, whereas GEPs have a spherical morphology. (Fig. 4(d))

The photoluminescence lifetime and PLQY of the synthesized multi-colored particles were investigated. As shown in Fig. 5, among the three different samples, GEPs have the longest PL lifetime estimated to be 1.52 μs . The second-longest lifetime was observed for BEPs with an average lifetime of 0.19 μs . Finally, YEP had the shortest lifetime estimated to be 0.0614 μs . The PLQYs of multi-colored perovskite nanoparticles were estimated and are presented in Table 2. Among the three different lead bromide materials, the GEPs had the highest PLQY of 66.6%, which was slightly lower than that of CsPbBr_3 reported previously, where it was estimated to range from 70% to 97% (Du *et al.* 2017, Shi *et al.* 2020). Moreover, PLQY of CsPbBr_3 were boosted up to approximately 100% by post surface treatment (Koscher *et al.* 2017). The anticipated lower PLQY may be caused by the incomplete

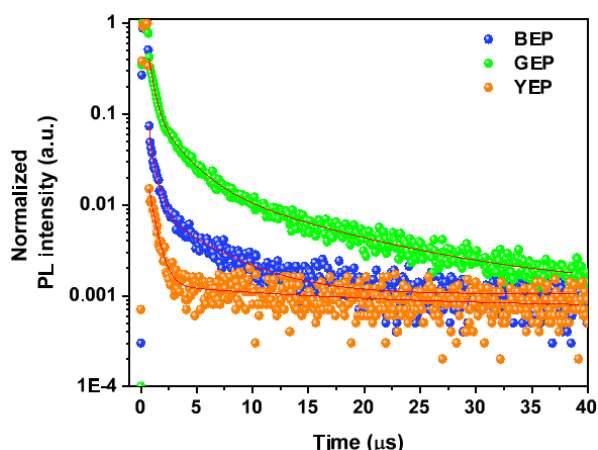


Fig. 5 Photoluminescence lifetime of BEPs, GEPs, and YEPs in the PVDF-HFP films

Table 2 Lifetime and PLQY of BEP, GEP, and YEP

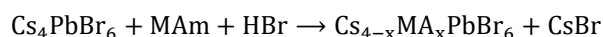
Material	λ_{ex} (nm)	λ_{em} (nm)	Lifetime (μ s)	PLQY (%)
BEP	370	450	0.135	49.4
GEP	370	521	1.520	66.6
YEP	520	550	0.061	32.8

transformation of CsPb_2Br_5 into CsPbBr_3 . On the other hand, the BEPs had a relatively good PLQY of 49.4% compared to the result of other studies (Zou *et al.* 2019). Finally, the YEPs had the lowest PLQY of 32.8%.

The surface chemistry of the BEPs, GEPs, and YEPs was explored by XPS analysis (Fig. 6). All three compounds exhibited two peaks for oxygen 1s at ~ 532 eV and ~ 533 eV. The peak located at ~ 532 eV is attributed to the C=O function of DMF, the presence of which was also confirmed by FTIR. In another report, the origin of the peak at ~ 532 eV was attributed to the PbCO_3 (Jana and Kim 2018). However, the absence of peaks on the Pb 4f spectrum corresponding to PbCO_3 at 139.3 and 144.2 eV indicates that PbCO_3 is not present. The second peak at ~ 533 eV corresponds to Pb(OH)_2 in BEP and GEP, whereas in YEP, this peak corresponds to PbBrOH . The Pb 4f_{7/2} and Pb 4f_{5/2} peaks appeared at 138.0 eV and 142.8 eV, respectively. Finally, the peaks of Br 3d at 67.95 eV and 68.93 eV correspond to Br 3d_{5/2} and Br 3d_{3/2}, respectively.

As mentioned above, many researchers have attempted to identify the solvent parameters that affect the synthesis of lead halide perovskites. Hamill *et al.* (2018) demonstrated that solvents with high D_N interact more strongly with Pb^{2+} ions, thus inhibiting the coordination of iodide, whereas solvents with low D_N interact weakly with the Pb^{2+} center, favoring the complexation of the lead cation with iodide. Based on the results of our characterizations and previously reported results, we hypothesized that the D_N of the solvents used in solvent blends is the main factor that predefines the structure of lead bromide particles. In this research, DMF ($D_N = 26.6$ kcal/mol) was mixed with three water-miscible solvents with different D_N values: DMSO (29.8 kcal/mol), isopropanol ($D_N = 21$ kcal/mol), and acetone ($D_N = 17$ kcal/mol). The solvent blend consisting of DMF and DMSO,

which has a high D_N , strongly coordinates with the Pb^{2+} center, thereby preventing the formation of lead bromide complexes and slowing down the crystallization of the perovskite. The long-term exposure of this mixture to methylamine, which subsequently transformed into methylammonium, resulted in the crystallization of the CsPbBr_3 perovskite. Moreover, the XRD results confirmed the formation of the CsPb_2Br_5 phase, which is subsequently transformed into CsPbBr_3 owing to the removal of PbBr_2 during immersion in water. The formation of CsPb_2Br_5 indicates the formation of PbBr_2 and PbBr_3^- complexes and once again confirms the proposed mechanism. On the other hand, the solvent blend consisting of DMF and isopropanol, which has a lower D_N , engages in comparatively less interaction with the Pb^{2+} center, thus favoring the formation of PbBr_6^{4-} octahedra. In the presence of the cation, the PbBr_6^{4-} octahedral complex recrystallizes to form the Ruddlesden–Popper perovskite based on lead bromide. However, formation of the Cs_4PbBr_6 phase requires Cs-rich conditions, which were impossible to establish in this synthesis method because of the equivalence of cesium and lead ions. Bearing in mind that the synthesis was performed under continuous methylamine vapor diffusion, which created MA^+ -rich conditions, we hypothesized that MA^+ promotes the formation of the Ruddlesden–Popper $\text{MA}_{4-x}\text{Cs}_x\text{PbBr}_6$ perovskite. To support our hypothesis, we performed density functional theory (DFT) simulations to investigate whether the MA^+ ion could be incorporated into Cs_4PbBr_6 with ease. As shown in Fig. 7, we substituted a single Cs^+ ion in the unit cell structure of Cs_4PbBr_6 (six formula units with an MA^+ ion). This enabled us to calculate the formation energy of the MA^+ defect, $\Delta E_f(\text{MA}^+)$, in consideration of the following reaction (here, $x = 1/6$ in our case):



$$\Delta E_f(\text{MA}^+) = E(\text{Cs}_{4-x}\text{MA}_x\text{PbBr}_6) + E(\text{CsBr}) - E(\text{Cs}_4\text{PbBr}_6) - E(\text{MAm}) - E(\text{HBr})$$

where MA_m represents the methylamine molecule, and the terms on the right-hand side are the total energies of MA^+ -doped Cs_4PbBr_6 , rock-salt CsBr, pure Cs_4PbBr_6 , and the methylamine and HBr molecules, respectively. The defect formation energy for the MA^+ substitutional defect was calculated to be -1.98 eV, meaning that the MA^+ ion would preferably be incorporated into the Cs_4PbBr_6 crystal as we proposed.

Finally, the blend consisting of DMF and acetone, which has the lowest D_N , undergoes very little interaction with the Pb^{2+} center, which results in the formation of PbBr_6^{4-} octahedra or $\text{Pb}_4\text{Br}_{11}^{3-}$ clusters in presence of acetone and Br-rich conditions. During the washing and precipitation step of YEP, lead bromide complexes are removed and transformed into CsPbBr_3 phase which was confirmed by XRD patterns.

To confirm the effect of the solvent, we performed the same reactions with other halides (Table 3). Interestingly, the replacement of lead bromide by lead iodide resulted in the formation of nanomaterials with a similar color trend but with very low photoluminescence efficiency, whereas

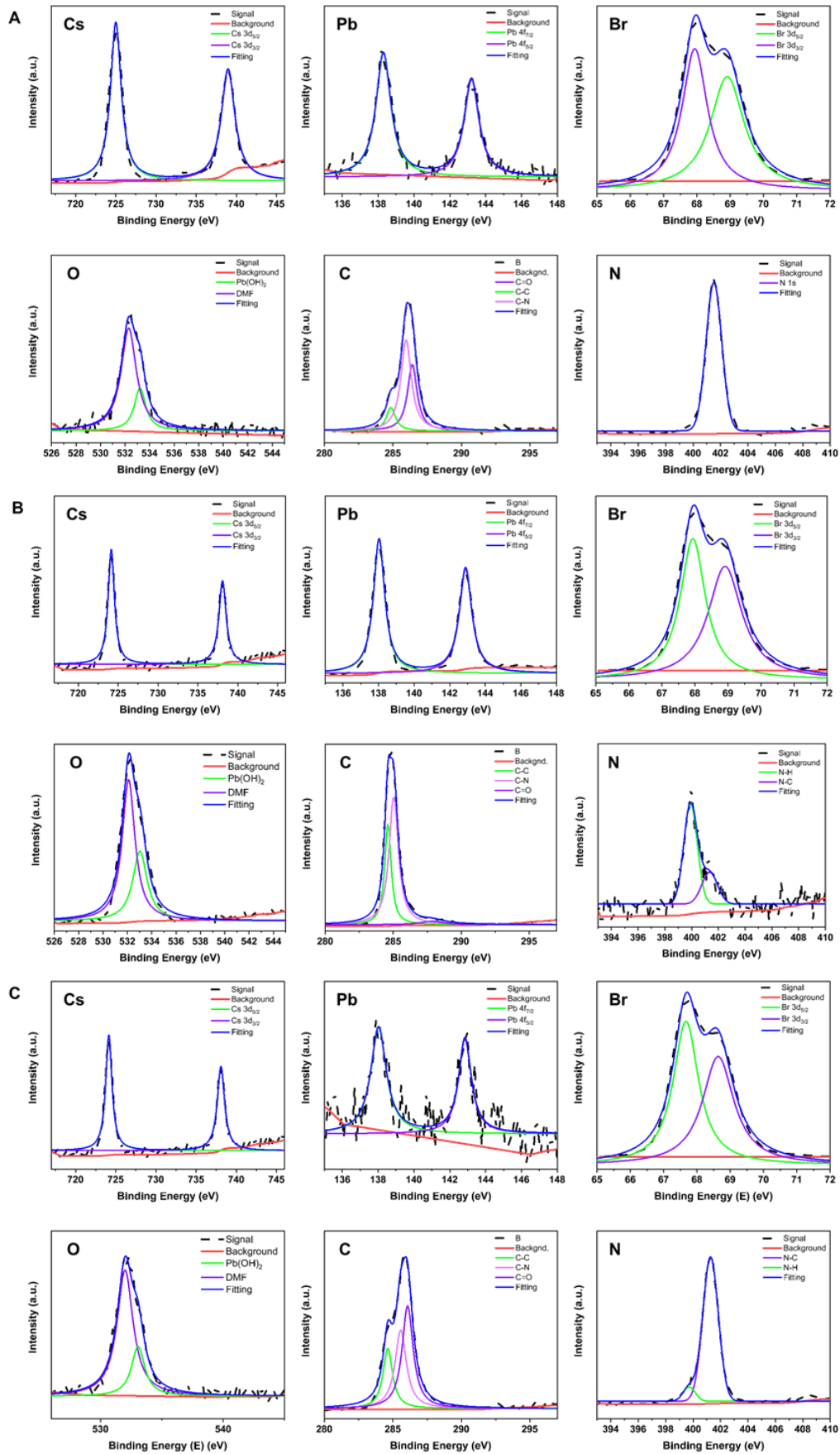


Fig. 6 XPS spectra of BEP, GEP, and YEP noted as (A), (B), and (C), respectively; The oxygen peak indicates the presence of Pb-O bonds in all these compounds

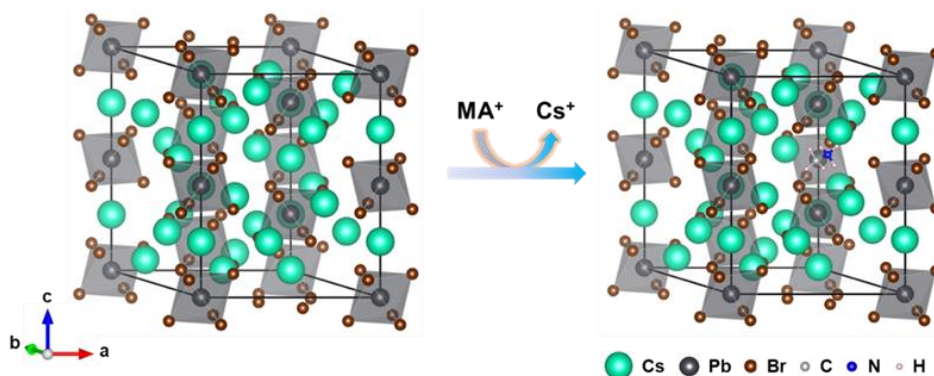


Fig. 7 Substitution of a single Cs^+ ion in the unit cell structure of Cs_4PbBr_6 to form $\text{Cs}_{4-x}\text{MA}_x\text{PbBr}_6$

Table 3 Preparation of perovskite with other halides

Big vials	Small vials	DMF	Acetone	DMSO	Isopropanol	Color
Vial 1 Chlorine	Sample 1	1 mL	0	0	3 mL	Blue
	Sample 2	1 mL	0	3 mL	0	No color
	Sample 3	1 mL	3 mL	0	0	Blue-Green
Vial 2 Iodine	Sample 1	1 mL	0	0	3 mL	Blue
	Sample 2	1 mL	0	3 mL	0	Green
	Sample 3	1 mL	3 mL	0	0	Blue-Orange

the replacement of lead bromide by lead chloride yielded different results. The lead chloride materials prepared in a mixture of DMF and DMSO did not undergo luminescence; however, the lead chloride materials prepared in blends of DMF/isopropanol and DMF/acetone emitted blue and blue-green fluorescent light, respectively. The observed difference may indicate that the Lewis basicity of halides may also be an essential factor for preparing lead halide perovskite materials.

4. Conclusions

In summary, a new approach for the synthesis of lead bromide, simultaneously controlling their phase, was developed by combining solvent blends and a prolonged LBVD system. In addition, the properties of the solvent blend play a crucial role in governing the formation of different lead bromide materials with different photoluminescent properties.

- Among the various solvent parameters, we found that the formation of different materials could most appropriately be explained in terms of the D_N .

- In contrast to previously reported work, we used blends of DMF with solvents with a variety of D_N values, which allowed slow recrystallization in the presence of methylamine vapor. Interestingly, the strength of the affinity for the Pb^{2+} center of solvents with different D_N values was found to be diverse, thus leading to the synthesis of various bromide perovskite nanomaterials.

- Moreover, the LBVD method allowed the perovskite materials to be protected by $\text{Pb}(\text{OH})_2$ and PbBrOH shells, which increased their stability in water to enhance their accessibility for various applications.

- Our study elucidated the importance of interactions among the Pb^{2+} center, solvents, and bromide ions during the synthesis of lead bromide perovskite nanomaterials. Further investigation with other halides and the characterization of the resulting materials is expected to provide insights into the effect of the Lewis basicity of halides. An improved understanding of the chemistry of the competition between the solvent and the halide to form a complex with the lead cation during the synthesis of perovskite materials is also anticipated.

Acknowledgments

This work was supported by the National Research Foundation of Korea (NRF) grant funded by the Korea government (MSIT) (2020R1A2C2007028 and 2020R1I1A3A04036531)

References

- Akkerman, Q.A., D’Innocenzo, V., Accornero, S., Scarpellini, A., Petrozza, A., Prato, M. and Manna, L. (2015), “Tuning the optical properties of cesium lead halide perovskite nanocrystals by anion exchange reactions”, *J. Am. Chem. Soc.*, **137**(32), 10276-10281. <https://doi.org/10.1021/jacs.5b05602>.
- Akkerman, Q.A., Park, S., Radicchi, E., Nunzi, F., Mosconi, E., De Angelis, F., Brescia, R., Rastogi, P., Prato, M. and Manna, L. (2017), “Nearly monodisperse insulator Cs_4PbX_6 (X = Cl, Br, I) nanocrystals, their mixed halide compositions and their transformation into CsPbX_3 nanocrystals”, *Nano Lett.*, **17**(3), 1924-1930. <https://doi.org/10.1021/acs.nanolett.6b05262>.
- Akkerman, Q.A., Abdelhady, A.L. and Manna, L. (2018), “Zero-dimensional cesium lead halides: History, properties and

- challenges”, *J. Phys. Chem. Lett.*, **9**(9), 2326-2337. <https://doi.org/10.1021/acs.jpcclett.8b00572>.
- Chin, S.H., Choi, J.W., Hu, Z., Mardegan, L., Sessolo, M. and Bolink, H.J. (2020), “Tunable luminescent lead bromide complexes”, *J. Mater. Chem. C*, **8**(45), 15996-16000. <https://doi.org/10.1039/D0TC04057F>.
- De Bastiani, M., Dursun, I., Zhang, Y., Alshankiti, B.A., Miao, X.H., Yin, J., Yengel, E., Alarousu, E., Turedi, B., Almutlaq, J.M., Saidaminov, M.I., Mitra, S., Gereige, I., AlSaggaf, A., Zhu, Y., Han, Y., Roqan, I.S., Bredas, J.L., Mohammed, O.F. and Bakr, O.M. (2017), “Inside perovskites: Quantum luminescence from bulk Cs₄PbBr₆ single crystals”, *Chem. Mater.*, **29**(17), 7108-7113. <https://doi.org/10.1021/acs.chemmater.7b02415>.
- Du, X., Wu, G., Cheng, J., Dang, H., Ma, K., Zhang, Y.W., Tan, P.F. and Chen, S. (2017), “High-quality CsPbBr₃ perovskite nanocrystals for quantum dot light-emitting diodes”, *RSC Adv.*, **7**(17), 10391-10396. <https://doi.org/10.1039/C6RA27665B>.
- Dutta, S.K. and Perkovic, M.W. (2002), “Lead as its own luminescent sensor”, *Inorg. Chem.*, **41**(26), 6938-6940. <https://doi.org/10.1021/ic0260724>.
- Fateev, S.A., Marchenko, E.I., Petrov, A.A., Goodilin, E.A. and Tarasov, A.B. (2020), “New acidic precursor and acetone-based solvent for fast perovskite processing via proton-exchange reaction with methylamine”, *Molecules*, **25**(8), 1856. <https://doi.org/10.3390/molecules25081856>.
- Giannozzi, P., Baroni, S., Bonini, N., Calandra, M., Car, R., Cavazzoni, C., Ceresoli, D., Chiarotti, G.L., Cococcioni, M., Dabo, I., Dal Corso, A., de Gironcoli, S., Fabris, S., Fratesi, G., Gebauer, R., Gerstmann, U., Gougoussis, C., Kokalj, A., Lazzeri, M., Martin-Samos, L., Marzari, N., Mauri, F., Mazzarello, R., Paolini, S., Pasquarello, A., Paulatto, L., Sbraccia, C., Scandolo, S., Sclauzero, G., Seitsonen, A.P., Smogunov, A., Umari, P. and Wentzcovitch, R.M. (2009), “Quantum espresso: A modular and open-source software project for quantum simulations of materials”, *J. Phys. Condens. Matter*, **21**(39), 395502. <https://doi.org/10.1088/0953-8984/21/39/395502>.
- Giannozzi, P., Andreussi, O., Brumme, T., Bunau, O., Buongiorno Nardelli, M., Calandra, M., Car, R., Cavazzoni, C., Ceresoli, D., Cococcioni, M., Colonna, N., Carnimeo, I., Dal Corso, A., de Gironcoli, S., Delugas, P., DiStasio, R.A., Ferretti, A., Floris, A., Fratesi, G., Fugallo, G., Gebauer, R., Gerstmann, U., Giustino, F., Gorni, T., Jia, J., Kawamura, M., Ko, H.Y., Kokalj, A., Küçükbenli, E., Lazzeri, M., Marsili, M., Marzari, N., Mauri, F., Nguyen, N.L., Nguyen, H.V., Otero-de-la-Roza, A., Paulatto, L., Poncé, S., Rocca, D., Sabatini, R., Santra, B., Schlipf, M., Seitsonen, A.P., Smogunov, A., Timrov, I., Thonhauser, T., Umari, P., Vast, N., Wu, X. and Baroni, S. (2017), “Advanced capabilities for materials modelling with quantum espresso”, *J. Phys. Condens. Matter*, **29**(46), 465901. <https://doi.org/10.1088/1361-648x/aa8f79>.
- Hamill, J.C., Schwartz, J. and Loo, Y.L. (2018), “Influence of solvent coordination on hybrid organic-inorganic perovskite formation”, *ACS Energy Lett.*, **3**(1), 92-97. <https://doi.org/10.1021/acscenergylett.7b01057>.
- Han, J., Sharipov, M., Hwang, S., Lee, Y., Huy, B.T. and Lee, Y.I. (2022), “Water-stable perovskite-loaded nanogels containing antioxidant property for highly sensitive and selective detection of roxithromycin in animal-derived food products”, *Sci. Rep.*, **12**(1), 3147. <https://doi.org/10.1038/s41598-022-07030-9>.
- Hu, H., Wu, L., Tan, Y., Zhong, Q., Chen, M., Qiu, Y., Yang, D., Sun, B., Zhang, Q. and Yin, Y. (2018), “Interfacial synthesis of highly stable CsPbX₃/oxide janus nanoparticles”, *J. Am. Chem. Soc.*, **140**(1), 406-412. <https://doi.org/10.1021/jacs.7b11003>.
- Huang, S., Li, Z., Kong, L., Zhu, N., Shan, A. and Li, L. (2016), “Enhancing the stability of CH₃NH₃PbBr₃ quantum dots by embedding in silica spheres derived from tetramethyl orthosilicate in “waterless” toluene”, *J. Am. Chem. Soc.*, **138**(18), 5749-5752. <https://doi.org/10.1021/jacs.5b13101>.
- Jana, A. and Kim, K.S. (2018), “Water-stable, fluorescent organic-inorganic hybrid and fully inorganic perovskites”, *ACS Energy Lett.*, **3**(9), 2120-2126. <https://doi.org/10.1021/acscenergylett.8b01394>.
- Jung, Y.K., Calbo, J., Park, J.S., Whalley, L.D., Kim, S. and Walsh, A. (2019), “Intrinsic doping limit and defect-assisted luminescence in Cs₄PbBr₆”, *J. Mater. Chem. A*, **7**(35), 20254-20261. <https://doi.org/10.1039/C9TA06874K>.
- Koscher, B.A., Swabeck, J.K., Bronstein, N.D. and Alivisatos, A.P. (2017), “Essentially trap-free CsPbBr₃ colloidal nanocrystals by postsynthetic thiocyanate surface treatment”, *J. Am. Chem. Soc.*, **139**(19), 6566-6569. <https://doi.org/10.1021/jacs.7b02817>.
- Kovalenko, M.V., Protesescu, L. and Bodnarchuk, M.I. (2017), “Properties and potential optoelectronic applications of lead halide perovskite nanocrystals”, *Science*, **358**(6364), 745-750. <https://doi.org/10.1126/science.aam7093>.
- Li, S.H., Chen, F.R., Zhou, Y.F. and Xu, J.G. (2009), “Pb₄Br₁₁³⁻ cluster as a fluorescent indicator for micro water content in aprotic organic solvents”, *Analyst*, **134**(3), 443-446. <https://doi.org/10.1039/B817787B>.
- Li, G., Rivarola, F.W.R., Davis, N.J.L.K., Bai, S., Jellicoe, T.C., de la Peña, F., Hou, S., Ducati, C., Gao, F., Friend, R.H., Greenham, N.C. and Tan, Z.K. (2016), “Highly efficient perovskite nanocrystal light-emitting diodes enabled by a universal crosslinking method”, *Adv. Mater.*, **28**(18), 3528-3534. <https://doi.org/10.1002/adma.201600064>.
- Li, F., Wang, H., Kufer, D., Liang, L., Yu, W., Alarousu, E., Ma, C., Li, Y., Liu, Z., Liu, C., Wei, N., Wang, F., Chen, L., Mohammed, O.F., Fratallocchi, A., Liu, X., Konstantatos, G. and Wu, T. (2017), “Ultra-high carrier mobility achieved in photoresponsive hybrid perovskite films via coupling with single-walled carbon nanotubes”, *Adv. Mater.*, **29**, 1602432. <https://doi.org/10.1002/adma.201602432>.
- Li, Z., Hu, Q., Tan, Z., Yang, Y., Leng, M., Liu, X., Ge, C., Niu, G. and Tang, J. (2018), “Aqueous synthesis of lead halide perovskite nanocrystals with high water stability and bright photoluminescence”, *ACS Appl. Mater. Interf.*, **10**(50), 43915-43922. <https://doi.org/10.1021/acsami.8b16471>.
- Lin, H., Zhang, X., Cai, L., Lao, J., Qi, R., Luo, C., Chen, S., Peng, H., Huang, R. and Duan, C. (2020), “High-stability fluorescent perovskites embedded in PbBrOH triggered by imidazole derivatives in water”, *J. Mater. Chem. C*, **8**(16), 5594-5599. <https://doi.org/10.1039/D0TC00939C>.
- Liu, Z., Bekenstein, Y., Ye, X., Nguyen, S.C., Swabeck, J., Zhang, D., Lee, S.T., Yang, P., Ma, W. and Alivisatos, A.P. (2017), “Ligand mediated transformation of cesium lead bromide perovskite nanocrystals to lead depleted Cs₄PbBr₆ nanocrystals”, *J. Am. Chem. Soc.*, **139**(15), 5309-5312. <https://doi.org/10.1021/jacs.7b01409>.
- Liu, K.K., Liu, Q., Yang, D.W., Liang, Y.C., Sui, L.Z., Wei, J.Y., Xue, G.W., Zhao, W.B., Wu, X.Y., Dong, L. and Shan, C.X. (2020), “Water-induced MAPbBr₃@PbBr(OH) with enhanced luminescence and stability”, *Light Sci. Appl.*, **9**(1), 44. <https://doi.org/10.1038/s41377-020-0283-2>.
- Loiudice, A., Saris, S., Oveisi, E., Alexander, D.T.L. and Buonsanti, R. (2017), “CsPbBr₃ QD/AlOx inorganic nanocomposites with exceptional stability in water, light and heat”, *Angew. Chem. Int. Ed.*, **56**(36), 10696-10701. <https://doi.org/10.1002/anie.201703703>.
- Nayak, P.K., Mahesh, S., Snaith, H.J. and Cahen, D. (2019), “Photovoltaic solar cell technologies: Analysing the state of the art”, *Nature Rev. Mater.*, **4**(4), 269-285. <https://doi.org/10.1038/s41578-019-0097-0>.
- Noel, N.K., Abate, A., Stranks, S.D., Parrott, E.S., Burlakov, V.M.,

- Goriely, A. and Snaith, H.J. (2014), "Enhanced photoluminescence and solar cell performance via lewis base passivation of organic-inorganic lead halide perovskites", *ACS Nano*, **8**(10), 9815-9821. <https://doi.org/10.1021/nn5036476>.
- Perdew, J.P., Ruzsinszky, A., Csonka, G.I., Vydrov, O.A., Scuseria, G.E., Constantin, L.A., Zhou, X. and Burke, K. (2008), "Restoring the density-gradient expansion for exchange in solids and surfaces", *Phys. Rev. Lett.*, **100**(13), 136406. <https://doi.org/10.1103/PhysRevLett.100.136406>.
- Quan, L.N., Quintero-Bermudez, R., Voznyy, O., Walters, G., Jain, A., Fan, J.Z., Zheng, X., Yang, Z. and Sargent, E.H. (2017), "Highly emissive green perovskite nanocrystals in a solid state crystalline matrix", *Adv. Mater.*, **29**(21), 1605945. <https://doi.org/10.1002/adma.201605945>.
- Rahimnejad, S., Kovalenko, A., Forés, S.M., Aranda, C. and Guerrero, A. (2016), "Coordination chemistry dictates the structural defects in lead halide perovskites", *ChemPhysChem*, **17**(18), 2795-2798. <https://doi.org/10.1002/cphc.201600575>.
- Rai, R.S. and Bajpai, V. (2021), "Recent advances in ZnO nanostructures and their future perspective", *Adv. Nano Res.*, **11**(1), 7. <https://doi.org/10.12989/anr.2021.11.1.037>.
- Riesen, N., Lockrey, M., Badek, K. and Riesen, H. (2019), "On the origins of the green luminescence in the "zero-dimensional perovskite" Cs₄PbBr₆: Conclusive results from cathodoluminescence imaging", *Nanoscale*, **11**(9), 3925-3932. <https://doi.org/10.1039/C8NR09255A>.
- Sadhanala, A., Deschler, F., Thomas, T.H., Dutton, S.E., Goedel, K.C., Hanusch, F.C., Lai, M.L., Steiner, U., Bein, T., Docampo, P., Cahen, D. and Friend, R.H. (2014), "Preparation of single-phase films of CH₃NH₃Pb(I_{1-x}Br_x)₃ with sharp optical band edges", *J. Phys. Chem. Lett.*, **5**(15), 2501-2505. <https://doi.org/10.1021/jz501332v>.
- Saidaminov, M.I., Abdelhady, A.L., Maculan, G. and Bakr, O.M. (2015), "Retrograde solubility of formamidinium and methylammonium lead halide perovskites enabling rapid single crystal growth", *Chem. Commun.*, **51**(100), 17658-17661. <https://doi.org/10.1039/C5CC00916E>.
- Sergeyev, D. (2021), "One-dimensional schottky nanodiode based on telescoping polyprismanes", *Adv. Nano Res.*, **10**(5), 471-479. <https://doi.org/10.12989/anr.2021.10.5.471>.
- Seth, S. and Samanta, A. (2017), "Fluorescent phase-pure zero-dimensional perovskite-related Cs₄PbBr₆ microdisks: Synthesis and single-particle imaging study", *J. Phys. Chem. Lett.*, **8**(18), 4461-4467. <https://doi.org/10.1021/acs.jpcllett.7b02100>.
- Shamsi, J., Urban, A.S., Imran, M., De Trizio, L. and Manna, L. (2019), "Metal halide perovskite nanocrystals: Synthesis, post-synthesis modifications and their optical properties", *Chem. Rev.*, **119**(5), 3296-3348. <https://doi.org/10.1021/acs.chemrev.8b00644>.
- Shi, S., Wang, Y., Zeng, S., Cui, Y. and Xiao, Y. (2020), "Surface regulation of CsPbBr₃ quantum dots for standard blue-emission with boosted PLQY", *Adv. Opt. Mater.*, **8**(12), 2000167. <https://doi.org/10.1002/adom.202000167>.
- Stevenson, J., Sorenson, B., Subramaniam, V.H., Raiford, J., Khlyabich, P.P., Loo, Y.L. and Clancy, P. (2017), "Mayer bond order as a metric of complexation effectiveness in lead halide perovskite solutions", *Chem. Mater.*, **29**(6), 2435-2444. <https://doi.org/10.1021/acs.chemmater.6b04327>.
- van Setten, M.J., Giantomassi, M., Bousquet, E., Verstraete, M.J., Hamann, D.R., Gonze, X. and Rignanese, G.M. (2018), "The pseudodojo: Training and grading a 85 element optimized norm-conserving pseudopotential table", *Comput. Phys. Commun.*, **226**, 39-54. <https://doi.org/10.1016/j.cpc.2018.01.012>.
- Wu, L., Hu, H., Xu, Y., Jiang, S., Chen, M., Zhong, Q., Yang, D., Liu, Q., Zhao, Y., Sun, B., Zhang, Q. and Yin, Y. (2017), "From nonluminescent Cs₄PbX₆ (X = Cl, Br, I) nanocrystals to highly luminescent CsPbX₃ nanocrystals: Water-triggered transformation through a CsX-stripping mechanism", *Nano Lett.*, **17**(9), 5799-5804. <https://doi.org/10.1021/acs.nanolett.7b02896>.
- Xing, G., Mathews, N., Sun, S., Lim, S.S., Lam, Y.M., Grätzel, M., Mhaisalkar, S. and Sum, T.C. (2013), "Long-range balanced electron- and hole-transport lengths in organic-inorganic CH₃NH₃PbI₃", *Science*, **342**(6156), 344-347. <https://doi.org/10.1126/science.1243167>.
- Xu, J., Huang, W., Li, P., Onken, D.R., Dun, C., Guo, Y., Ucer, K.B., Lu, C., Wang, H., Geyer, S.M., Williams, R.T. and Carroll, D.L. (2017), "Imbedded nanocrystals of cspbbr₃ in Cs₄PbBr₆: Kinetics, enhanced oscillator strength and application in light-emitting diodes", *Adv. Mater.*, **29**(43), 1703703. <https://doi.org/10.1002/adma.201703703>.
- Xuan, T., Lou, S., Huang, J., Cao, L., Yang, X., Li, H. and Wang, J. (2018), "Monodisperse and brightly luminescent CsPbBr₃/Cs₄PbBr₆ perovskite composite nanocrystals", *Nanoscale*, **10**(21), 9840-9844. <https://doi.org/10.1039/C8NR01266K>.
- Yamanouchi, J., Oku, T., Ohishi, Y., Fukaya, M., Ueoka, N., Tanaka, H. and Suzuki, A. (2018), "Fabrication and characterization of perovskite CH₃NH₃Pb_{1-x}Sb_xI_{3-3x}Br_{3x} photovoltaic devices", *Adv. Mater. Res.*, **7**(1), 73-81. <https://doi.org/10.12989/amr.2018.7.1.073>.
- Yin, J., Yang, H., Song, K., El-Zohry, A.M., Han, Y., Bakr, O.M., Brédas, J.L. and Mohammed, O.F. (2018), "Point defects and green emission in zero-dimensional perovskites", *J. Phys. Chem. Lett.*, **9**(18), 5490-5495. <https://doi.org/10.1021/acs.jpcllett.8b02477>.
- Ying, G., Jana, A., Osokin, V., Farrow, T., Taylor, R.A. and Park, Y. (2020), "Highly efficient photoluminescence and lasing from hydroxide coated fully inorganic perovskite micro/nano-rods", *Adv. Opt. Mater.*, **8**(23), 2001235. <https://doi.org/10.1002/adom.202001235>.
- Yoon, S.J., Draguta, S., Manser, J.S., Sharia, O., Schneider, W.F., Kuno, M. and Kamat, P.V. (2016), "Tracking iodide and bromide ion segregation in mixed halide lead perovskites during photoirradiation", *ACS Energy Lett.*, **1**(1), 290-296. <https://doi.org/10.1021/acsenerylett.6b00158>.
- Zhong, Q., Cao, M., Hu, H., Yang, D., Chen, M., Li, P., Wu, L. and Zhang, Q. (2018), "One-pot synthesis of highly stable CsPbBr₃@SiO₂ core-shell nanoparticles", *ACS Nano*, **12**(8), 8579-8587. <https://doi.org/10.1021/acsnano.8b04209>.
- Zou, Y., Xu, H., Li, S., Song, T., Kuai, L., Bai, S., Gao, F. and Sun, B. (2019), "Spectral-stable blue emission from moisture-treated low-dimensional lead bromide-based perovskite films", *ACS Photonics*, **6**(7), 1728-1735. <https://doi.org/10.1021/acsp Photonics.9b00435>.